An MPC Strategy for Low-Thrust Space Debris Rendezvous

Mirko Leomanni, Gianni Bianchini, Andrea Garulli, Antonio Giannitrapani, Renato Quartullo

***Abstract*— The removal of orbital debris by means of dedicated space missions has been recently identified as a priority for the sustainability of the space environment. Electrically propelled spacecraft, in particular, are seen as a cost-effective solution for such type of missions. This paper develops an MPC strategy for space debris rendezvous, which is able to account for mission-specific performance and safety requirements, while satisfying on-off constraints inherent to the electric propulsion technology. The proposed design requires to solve a mixed integer linear program at each time step. In order to limit the computational burden, a linear programming relaxation tailored to a realistic thrusting configuration is devised. A rendezvous case study demonstrates the effectiveness of the proposed solution.**

I. Introduction

An impressive amount of space debris such as discarded rocket stages, defunct satellites, and small fragments generated by explosions, is orbiting the Earth. The debris density in the Low Earth Orbit (LEO) regime is currently so high that there is a tangible threat of frequent collisions becoming a reality. Experts in the field have warned that a cascade of collisions would lead to an exponential growth of the number of debris fragments, which may jeopardize future space activities [1], [2]. Motivated by such concerns, major space agencies have identified active debris removal as an essential risk mitigation approach [3], [4].

Active debris removal missions are composed of different phases: a servicing spacecraft must first approach a target debris, bring it to a lower altitude orbit and then, in case of a multi-target mission, repeat the whole process. Due to the large velocity changes (delta-v) involved in this process, the design of these missions is subject to stringent constraints. In particular, the amount of debris objects which can be de-orbited is heavily dependent on the fuel efficiency of the propulsion system. In this respect, electric propulsion (EP) is seen as a key technology for reducing propellant consumption, thus enabling the removal of multiple debris targets within a single mission [5]. Despite its efficiency, the EP technology is inherently low thrust and thus it can provide only a limited control authority. This limitation must be carefully addressed in the control design problem, especially for applications requiring a high degree of autonomy.

Achieving autonomous orbital rendezvous is among the key technological challenges for space debris removal. In this respect, the development of suitable feedback control techniques plays a pivotal role [6], [7], [8]. Model predictive control (MPC) has proven to be particularly well-suited, due to its ability to optimize relevant performance indexes while enforcing thrust and maneuver safety constraints [9]. State-of-the-art MPC design methodologies for the rendezvous problem are documented in a vast body of literature, see, e.g., [10], [11], [12], [13], [14]. However, in most of the related works the technological limitations of low-thrust propulsion are addressed only marginally. In particular, the fact that many EP engines must be operated in on-off mode (see, e.g., [15], [16]) is typically overlooked.

In this paper, an MPC strategy is presented for space debris rendezvous with low-thrust propulsion. The proposed design allows one to trade-off fuel consumption and state regulation performance, while accounting for mission-specific safety and propulsion requirements. On-off constraints dictated by the EP technology are embedded directly in the MPC problem formulation, by adopting a mixed integer linear programming (MILP) framework. In order to limit the computational burden, a linear programming (LP) relaxation tailored to the thrusting configuration is devised. A detailed analysis of the control system performance is presented for a rendezvous case study involving a debris object in LEO.

The paper is organized as follows. The debris rendezvous problem is introduced in Section II. A linearized relative motion model suitable for this problem is presented in Section III. Section IV describes the proposed MPC strategy. The rendezvous case study is discussed in Section V, and conclusions are drawn in Section VI.

Notation: In this paper, three coordinate frames are used. The first one is the Earth-Centered-Inertial (ECI) frame, whose fundamental plane is the Earth's equatorial plane. Its axes are denoted by X_I, Y_I and Z_I. The second one is a Radial-Transverse-Normal (RTN) frame centered at the spacecraft. The R-axis is aligned to the position vector joining the Earth and the spacecraft, the N-axis points towards the orbit normal, and the T-axis completes a right handed triad. The third coordinate frame is the so-called spacecraft body frame, whose axes X_b, Y_b and Z_b are rigidly attached to the spacecraft bus.

II. Space Debris Rendezvous

In space debris removal missions, a maneuvering spacecraft is required to rendezvous a pre-selected debris object and capture it with a dedicated device. The debris is then de-orbited by activating a suitable propulsion module, such as EP. The availability of a high-efficiency, low-thrust EP system on board the spacecraft may also be exploited in order to lower the amount of propellant needed to safely rendezvous with the debris, a possibility which is explored in this paper. The considered scenario is as follows. At the beginning of the rendezvous process, the spacecraft travels along an orbit with approximately the same orientation and

The authors are with the Dipartimento di Ingegneria dell'Informazione e Scienze Matematiche, Università di Siena, Siena, Italy. Email: : {leomanni,giannibi,garulli,giannitrapani}@dii.unisi.it

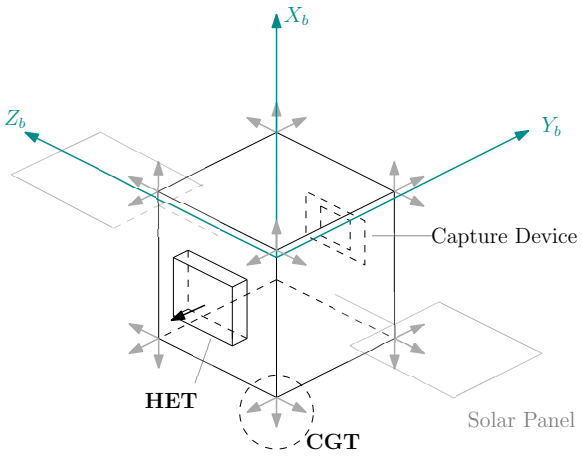

Fig. 1. Spacecraft layout.

an altitude slightly lower than that of the target debris. Although the two orbits are close to each other, the initial phase error between the spacecraft and the target can be quite large, resulting in a large initial inter-satellite separation (in the order of, e.g., 10^3 km). Rendezvous operations are typically split into multiple stages, depending on the actual inter-satellite separation. We consider two consecutive stages: *phasing* and *terminal rendezvous* (see, e.g., [17]). In the phasing stage, the spacecraft must reach a *holding point* situated a few kilometers away from the target, along the target orbit. The major requirement in this stage is to perform the maneuver in a fuel-efficient manner. In the terminal rendezvous stage, a second maneuver is performed, which brings the spacecraft from the holding point to a *capture point* much closer to the target (e.g., 1 m). At this point, the debris capture device is activated. An important safety requirement for terminal rendezvous is to avoid potential collisions.

The spacecraft layout is depicted in Fig. 1. An EP module consisting of a single Hall Effect Thruster (HET) is considered as the primary actuation device. It is located on a side of the spacecraft and aligned to the direction Y_b of the body frame. The propulsion system design is complemented by a set of 24 cold gas micro-thrusters (CGTs) organized in orthogonal triads centered at the bus vertices. These are operated in groups of four to provide decoupled control forces along the three basis vectors of the body frame, while minimizing the torque generated about the spacecraft center of mass. CGTs pointing in opposite directions are never fired simultaneously. The maximum thrust delivered by the CGTs is usually much higher than the thrust provided by the HET, albeit their fuel efficiency is nearly two orders of magnitude lower. The debris capture device is mounted on the opposite side of the HET. Such a configuration is taken into account for rendezvous maneuver planning. Debris capture and de-orbiting operations are not addressed in this work.

III. Relative motion dynamics

In this section, a linearized model of the relative motion between two satellites which is suitable for the considered

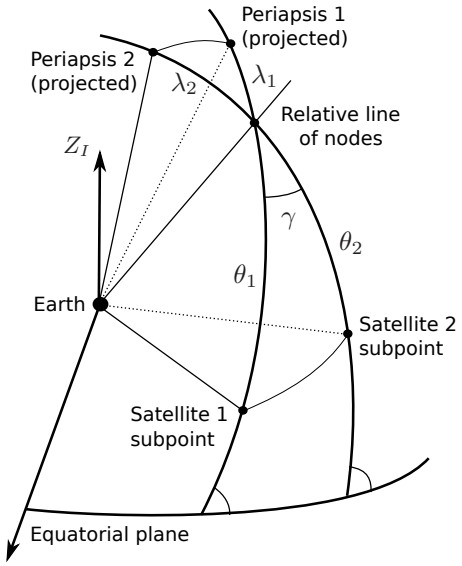

Fig. 2. Relative motion geometry on the unit sphere

rendezvous problem is presented. Let us refer to the debris and the spacecraft as satellites 1 and 2, respectively. Define the *relative line of nodes* as intersection of the orbital planes of the two satellites. Moreover, denote by γ the angle between the two orbital planes and by λ_j, θ_j the angles formed by the orbit periapses and by the satellite position vectors with respect to the relative line of nodes, see Fig. 2. The relationship between these angles and classical orbital elements is described in detail in [18].

The relative motion error is parameterized by the state vector $x = [x_1, \ldots, x_6]^T$, defined by

$$\begin{aligned} x_1 &= \theta_2 - (\theta_1 + \phi) \\ x_2 &= (n_2 - n_1)/n_1 \\ x_3 &= e_2 \cos(\theta_2 - \lambda_2) - e_1 \cos(\theta_2 - \lambda_1) \\ x_4 &= e_2 \sin(\theta_2 - \lambda_2) - e_1 \sin(\theta_2 - \lambda_1) \\ x_5 &= \tan(\gamma/2) \cos\theta_2 \\ x_6 &= \tan(\gamma/2) \sin\theta_2, \end{aligned} \tag{1}$$

where n_j, e_j are the mean motion and the eccentricity of satellite j, respectively, and ϕ defines the phase offset between satellite 1 (the debris) and either the capture or the holding point, depending on the maneuvering stage. When $x = 0$, the two satellites are guaranteed to follow exactly the same orbital path, with a relative phase angle equal to ϕ.

We restrict our attention to rendezvous maneuvers involving near-circular orbits (most debris objects lie in this type of orbit, see, e.g., [5]). A point-mass gravity model is considered for control design. Within this setting, the linearized dynamics of the state vector (1) take on the form (see [19], in which a similar model is derived)

$$\dot{x} = A_c\, x + B_c\, u, \tag{2}$$

where $\dot{x} = \mathrm{d}x/(\mathrm{d}n_1 t)$ denotes the derivative of vector x with

respect to the scaled time $n_1 t$, and

$$A_c = \begin{bmatrix} 0 & 1 & 2 & 0 & 0 & 0 \\ 0 & 0 & 0 & 0 & 0 & 0 \\ 0 & 0 & 0 & -1 & 0 & 0 \\ 0 & 0 & 1 & 0 & 0 & 0 \\ 0 & 0 & 0 & 0 & 0 & -1 \\ 0 & 0 & 0 & 0 & 1 & 0 \end{bmatrix}, \; B_c = \begin{bmatrix} 0 & 0 & 0 \\ 0 & -3 & 0 \\ 0 & 2 & 0 \\ 1 & 0 & 0 \\ 0 & 0 & 1/2 \\ 0 & 0 & 0 \end{bmatrix}.$$

The input vector u in (2) is related to the control force F delivered by satellite 2 (the controlled spacecraft), expressed in the RTN frame, by the identity

$$\beta\, u = F/m_2 \tag{3}$$

where $\beta = n_1(\mu\, n_1)^{1/3}$ is a positive constant, m_2 is the mass of satellite 2, and μ denotes the gravitational parameter.

Model (2)-(3) provides a general description of the motion of a controlled spacecraft relative to an uncontrolled reference, in the neighborhood of a circular orbit. The size of the reference orbit is embedded in the scaled time variable $n_1 t$ and in the scaling parameter β. Similarly to what observed in [19], the model is valid even for large along-track separations.

IV. Rendezvous Control Problem

For the purpose of digital control design, system (2) is discretized with a sampling interval τ_s by using a zero-order hold on the control input, resulting in the discrete-time model

$$x(k+1) = A\, x(k) + B\, u(k). \tag{4}$$

The dimensional unit of τ_s is radians per sample, where 2π radians correspond to a full orbital period of the target debris. The considered rendezvous control problem is that of steering system (4) to the origin, while avoiding collisions and satisfying thrust constraints specific to the HET and CGT technologies. In this regard, it should be noticed that both HET and CGT engines are commonly operated in on-off mode. However, while the HET pulse modulation frequency is typically of the same order of magnitude as the control bandwidth, CGTs are usually paired with a dedicated pulse-width modulator operating at a much higher frequency, where the input to the modulator is a continuous signal evolving on the same time scale as the feedback loop. Accordingly, and considering the discretization (4), the HET control command is assumed to be binary, while that of the CGT system is assumed to be a variable amplitude one. The design of a suitable CGT modulation system is not covered in this paper. In the following, an MPC strategy is proposed for the rendezvous problem.

A. Thrust Constraints

The CGT units in Fig. 1 are modeled as a single actuation system able to produce thrust in the three directions of the body frame. During rendezvous operations, the body frame is nominally aligned to the RTN frame (in particular, the Y_b-axis is aligned with the T-axis). Consequently, the control input $u(k)$ in (4) takes on the form

$$u(k) = u_C(k) + \begin{bmatrix} 0 & s\, u_H(k) & 0 \end{bmatrix}^T \tag{5}$$

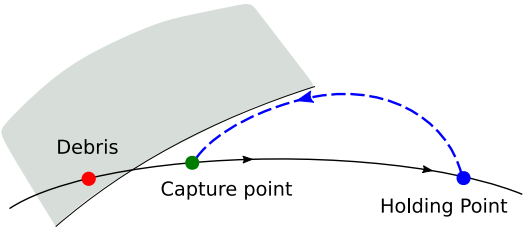

Fig. 3. Illustration of the state constraint (8) for $\gamma = 0$: the forbidden zone is greyed out.

where $u_C(k)$ and $u_H(k)$ correspond to the accelerations generated by the CGT and HET engines, respectively. The scalar parameter s in (5) takes values $+1$ or -1 depending on whether Y_b (and hence the HET thrust vector, see Fig. 1) points towards the positive or negative T-axis direction. In this work, we set $s = 1$ in the phasing stage and $s = -1$ in the terminal rendezvous stage.

Thrust limitations are modeled by the following constraints

$$\|u_C(k)\|_\infty \leq \frac{F_C}{\beta m_2} \tag{6}$$

$$u_H(k) \in \left\{0, \frac{F_H}{\beta m_2}\right\} \tag{7}$$

where F_C and F_H denote the maximum thrust of the CGT system and of the HET, respectively (see (3)). According to the considered thruster technologies, $F_H \ll F_C$. The feasible input set (6) for the CGT system is a box, because the CGT propulsion units are aligned with the RTN axes, while the constraint (7) describes the on-off nature of the HET. Further constraints can be included in the control requirements, such as the limitation of the number of thruster firings, but are not addressed here for the sake of brevity.

B. Safety Constraints

In the terminal rendezvous stage, maneuver safety requirements are taken into account by means of a constraint taking the form

$$c_1\, x_1(k) + c_2 \frac{\delta r(k)}{a_1} \leq d \tag{8}$$

where c_1, c_2 and d are constant parameters, $a_1 = \mu^{1/3}\, n_1^{-2/3}$ is the target semi-major axis value, and $\delta r(k)$ denotes the difference in orbit radius between the spacecraft and the target at step k. The boundary of the inequality (8) separates an admissible (i.e., safe) region for the controlled spacecraft from another one containing the target debris, in which collisions might occur (see, e.g., Fig. 3). By using (1), the orbit radius equation, and the fact that the target orbit is approximately circular, one can express $\delta r(k)$ in (8) as

$$\delta r(k) = a_1 \left\{ \frac{1 - x_3^2(k) - x_4^2(k)}{[1 + x_3(k)]\,[1 + x_2(k)]^{\frac{2}{3}}} - 1 \right\}. \tag{9}$$

The relative states (1) lie in a small neighborhood of the origin during terminal rendezvous. Thus, (8)-(9) can be approximated by its linearized counterpart. Linearizing (8)-(9) about $x = 0$ results in

$$c_1\, x_1(k) - \frac{2c_2}{3}\, x_2(k) - c_2\, x_3(k) \leq d. \tag{10}$$

The constraint (10) is employed to make the spacecraft follow a predefined glide slope towards the target, so as to avoid collisions, while ensuring that the target remains within the field of view of the navigation instruments installed onboard the spacecraft.

C. MPC Scheme

The rendezvous control system must provide a compromise between fuel consumption and state regulation performance. Over a time period containing a given number N of consecutive discrete-time samples, the fuel consumption is proportional to

$$\sum_{k=0}^{N-1} \frac{\|u_C(k)\|_1}{Isp_C} + \frac{u_H(k)}{Isp_H}, \tag{11}$$

where Isp_C and Isp_H denote the specific impulse of the CGT and HET systems, respectively. As a measure of state regulation performance, we define the cost $\sum_{k=0}^{N-1} \|Q\,x(k)\|_1$ where Q is a full rank weighting matrix. The adoption of the ℓ_1-norm allows one to formulate the control problem via linear programming techniques. Thus, the cost function to be minimized can be defined as

$$\sum_{k=0}^{N-1} \|Q\,x(k)\|_1 + \|u_C(k)\|_1 + r\,u_H(k), \tag{12}$$

where $r = Isp_C/Isp_H$. Note that $r \ll 1$.

In order to satisfy the control requirements (6)-(7) and (10), while minimizing (12), the following optimization problem is formulated

$$\begin{aligned}
\min_{\hat{U}_C,\,\hat{U}_H} \; & \sum_{j=0}^{N-1} \|Q\,\hat{x}(j)\|_1 + \|\hat{u}_C(j)\|_1 + r\,\hat{u}_H(j) \\
\text{s.t.} \quad & \hat{x}(j+1) = A\,\hat{x}(j) + B\,\hat{u}(j) \\
& \hat{u}(j) = \hat{u}_C(j) + \begin{bmatrix} 0 & s\,\hat{u}_H(j) & 0 \end{bmatrix}^T \\
& \|\hat{u}_C(j)\|_\infty \le F_C/(\beta m_2) \\
& \hat{u}_H(j) \in \{0, F_H/(\beta m_2)\} \\
& c_1\,\hat{x}_1(j) - 2c_2\,\hat{x}_2(j)/3 - c_2\,\hat{x}_3(j) \le d \\
& \hat{x}(0) = x(k), \;\; \hat{x}(N) = 0,
\end{aligned} \tag{13}$$

where the decision variables are the control sequences

$$\hat{U}_C = \{\hat{u}_C(0), \ldots, \hat{u}_C(N-1)\} \tag{14}$$

$$\hat{U}_H = \{\hat{u}_H(0), \ldots, \hat{u}_H(N-1)\}, \tag{15}$$

and s is fixed according to the maneuvering stage (see Section IV-A). The MPC strategy amounts to solving problem (13) at each discrete time step k and applying the control input

$$u(k) = \hat{u}(0) = \hat{u}_C(0) + \begin{bmatrix} 0 & s\,\hat{u}_H(0) & 0 \end{bmatrix}^T \tag{16}$$

to system (4). Closed-loop exponential stability is guaranteed by the terminal constraint $\hat{x}(N) = 0$, see [20]. Since $r \ll 1$, the control policy (13)-(16) promotes HET firings as opposed to CGT ones. In other words, CGTs are employed only when a fine tuning of the control action is needed, or when the thrust delivered by the HET is not sufficient to achieve the state regulation objective.

Problem (13) can be cast as a MILP, in which N binary variables are used to model the control sequence (15). The computational complexity of this approach is known to scale badly with the length N of the prediction horizon. In order to mitigate this issue, a suitable relaxation is proposed, which exploits the flexibility of the spacecraft propulsion system layout. Specifically, the binary constraint $\hat{u}_H(j) \in \{0,\, F_H/(\beta m_2)\}$ in (13) is replaced by the linear inequality

$$0 \le \hat{u}_H(j) \le F_H/(\beta m_2). \tag{17}$$

The resulting optimization problem can be solved as a standard LP, for which computationally efficient tools are available. The first elements of the control sequences provided by the LP solution at step k are denoted by $\hat{u}'_C$ and $\hat{u}'_H$. Most of the time, the HET input $\hat{u}'_H$ still meets the original binary constraint, since ℓ_1-norm minimization promotes the operation of the actuators at the boundary of the feasible input set (see, e.g., [21]). However, this is not always guaranteed.

An effective approach to address this issue is to set the actual HET command either to 0 or to $u_M = F_H/(\beta m_2)$, based on whether $\hat{u}'_H$ exceeds a predefined threshold q, and to compensate for the difference in the overall control action by using the CGT system. Formally, this amounts to choose the actual actuator commands as

$$\begin{cases} u_C(k) = \hat{u}'_C + \begin{bmatrix} 0 & s(\hat{u}'_H - u_M) & 0 \end{bmatrix} \\ u_H(k) = u_M \end{cases} \quad \text{if } \; q \le \hat{u}'_H \le u_M$$

$$\begin{cases} u_C(k) = \hat{u}'_C + \begin{bmatrix} 0 & s\,\hat{u}'_H & 0 \end{bmatrix} \\ u_H(k) = 0 \end{cases} \quad \text{if } \; 0 \le \hat{u}'_H < q. \tag{18}$$

The control allocation scheme (18) satisfies (7) by construction. Moreover, it also satisfies (6). In fact, by optimality of the solution of the relaxed problem, the second entry of $\hat{u}'_C$ cannot take opposite sign to that of $s\,\hat{u}'_H$, and must be equal to zero when $0 < \hat{u}'_H < u_M$ (recall that $r < 1$ in (12)). By using this property in (18) and taking into account that $\|\hat{u}'_C\|_\infty \le F_C/(\beta m_2)$, $u_M < F_C/(\beta m_2)$, one can verify that the constraint (6) is met. Clearly, the control input (5) resulting from (18) is exactly equal to that obtained by solving the LP and then applying $u(k) = \hat{u}' = \hat{u}'_C + [0 \;\; s\,\hat{u}'_H \;\; 0]^T$. Notice that the latter control is exponentially stabilizing, thanks to the terminal constraint $\hat{x}(N) = 0$. Thus, exponential stability holds also for the control policy (18). In order to find a suitable value of q , we minimize the instantaneous fuel consumption $\|u_C(k)\|_1 + r\,u_H(k)$ resulting from (18). This gives $q = (r+1)u_M/2$.

V. Rendezvous Case Study

A simulation case study of the rendezvous scenario described in Section II is presented. The target debris element is a non-operational satellite on an orbit with the following characteristics: semi-major axis equal to 7378 km, eccentricity of 0.001 and inclination of 81 deg. The wet mass of

the servicing spacecraft is 100 kg. The maximum deliverable thrust is $F_H = 15$ mN for the HET and $F_C = 150$ mN for the CGT system, while their specific impulses are $Isp_H = 1200$ s and $Isp_C = 30$ s, according to the specifications of such devices [22]. The rendezvous maneuver is simulated by using a nonlinear truth model accounting for Earth asphericity, atmospheric drag, luni-solar gravity, and solar radiation pressure perturbations. The relative state vector (1) is computed from the mean orbital elements of the spacecraft and the target. Simulation results are reported below for each of the two stages of the rendezvous process.

Phasing: At the beginning of the simulation, the servicing spacecraft is orbiting 12 km below the target debris, out-of-phase by -0.068 rad. The initial inter-satellite separation amounts to approximately 500 km. In the phasing stage, one has that $s = 1$ in (5). The maneuver objective is to steer the spacecraft towards the holding point defined by $\phi = 2.7 \cdot 10^{-4}$ rad in (1), located 2 km ahead of the target. This is achieved by exploiting the control policy (18). The sampling interval and the MPC prediction horizon are taken as $\tau_s = \pi/8$ (corresponding to approximately 6 minutes) and $N = 128$, respectively. A trial and error procedure is adopted to tune the weighting matrix Q in (13), so as to trade-off fuel expenditure and state regulation performance, yielding $Q = 10^{-2} \cdot \text{diag}(0.05, 1, 1, 1, 7, 7)$. The LP-relaxed MPC problem is solved by using the commercial package Gurobi. On a standard laptop, the computation time is in the order of 1 s, i.e., a negligible fraction of the sampling time. Figure 4 depicts the evolution of the satellite relative radius versus the along-track (phase) separation. It can be seen that the holding point position is successfully acquired. Figure 5 shows the thruster commands (the radial CGT component is null and thus omitted). These satisfy the input constraints (6)-(7). As expected, tangential (T-axis) thrusting is performed by firing mainly the HET, in order to contain as much as possible the fuel consumption, while the tangential CGT component is used just to fine-tune the control action. Moreover, tangential control turns out to be idle during the first simulation hour, which favours a natural drift of the relative phase. The normal (N-axis) CGT component is used to compensate for an initial misalignment of $\gamma = 5.2 \cdot 10^{-4}$ rad between the two satellite orbital planes. In this mission stage, the adoption of the HET allows one to save approximately 1.9 kg of propellant compared to using the CGT system alone. Considering that in multi-debris removal missions phasing operations must be repeated multiple times, this is a significant figure.

Terminal Rendezvous: Once the holding point is acquired, the spacecraft is rotated so as to point the relative motion sensors and the capture device towards the target debris, resulting in $s = -1$ in (5). The terminal rendezvous maneuver is then initiated, with the objective of reaching the capture point defined by $\phi = 2 \cdot 10^{-7}$ rad in (1), located 1.5 m ahead of the target. The mixed-integer MPC scheme (13)-(16) is adopted to this purpose. The sampling interval and the prediction horizon are set as $\tau_s = \pi/16$ and $N = 32$, respectively. The same weighting matrix Q adopted for the phasing maneuver is used. The parameters c_1, c_2 and d in

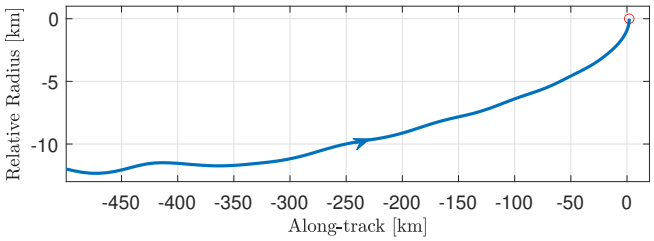

Fig. 4. Relative radius δr versus along-track separation $a_1\ (\theta_2 - \theta_1)$ during the acquisition of the holding point (circled).

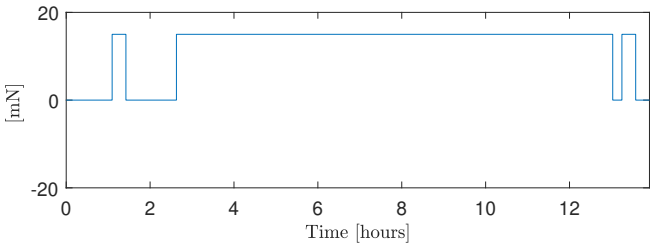

(a) HET ($s\beta m_2 u_H$)

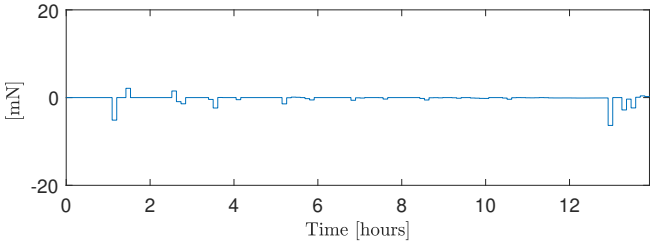

(b) CGTs, tangential direction

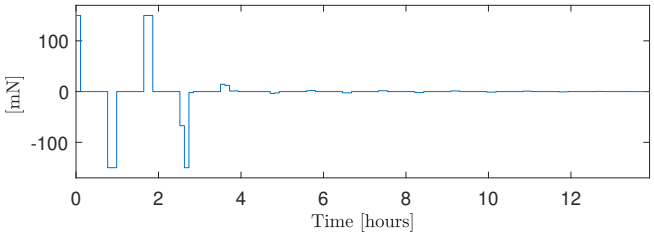

(c) CGTs, normal direction

Fig. 5. Thrust profiles in the phasing stage.

(10) are tuned so as to guarantee that the relative elevation angle between the spacecraft and the debris, measured with respect to the local horizontal, will not exceed 30 deg. This value is compatible with the field of view of the optical instruments commonly employed for relative navigation. The Gurobi solver time for the MILP problem amounts on average to 0.6 s. Figure 6 shows the radial versus tangential displacement between the spacecraft and the debris, together with the profile of the state constraint (10). It can be seen that the MPC scheme is able to meet this constraint, thus ensuring maneuver safety. The thruster commands are depicted in Fig. 7 (the normal CGT component is null and thus omitted) and satisfy (6)-(7). The initial peaks in the CGT command profiles provide the control authority necessary to reach the capture point while enforcing (10).

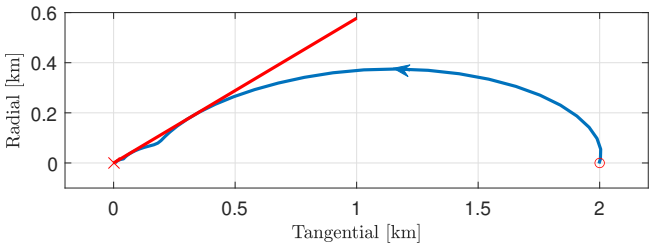

Fig. 6. Spacecraft trajectory (blue) and state constraint boundary (red), in the terminal rendezvous stage.

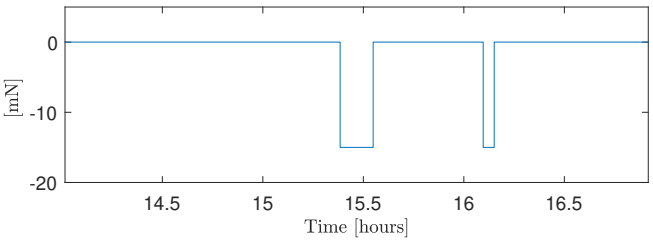

(a) HET ($s\beta m_2 u_H$)

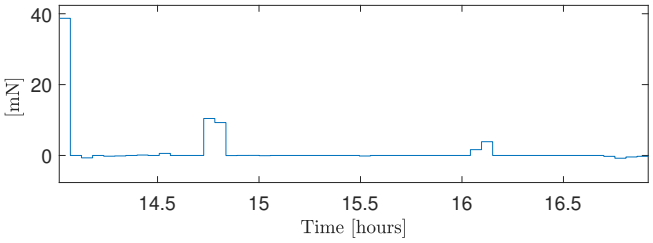

(b) CGTs, tangential direction

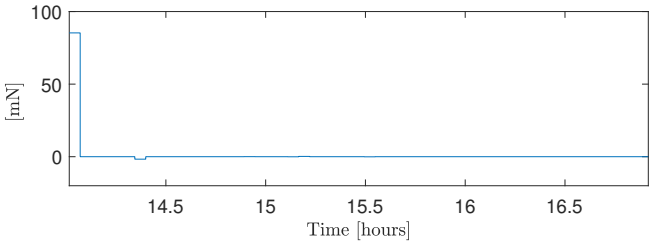

(c) CGTs, radial direction

Fig. 7. Thrust profiles in the terminal rendezvous stage.

VI. Conclusions

A model predictive control strategy has been presented for space debris rendezvous with low-thrust propulsion. Besides ensuring maneuver safety, the proposed design allows one to effectively deal with the specific technological limitations of the propulsion technology. The control strategy has been tested on a rendezvous case study involving a debris object in Low Earth Orbit. Simulation results show that the rendezvous objective is achieved safely and autonomously, while making an efficient use of the available propulsion resources. Future research will address further important aspects of the mission design, such as a detailed modeling of debris capture and de-orbiting operations.

References

[1] J.-C. Liou and N. L. Johnson, "Instability of the present LEO satellite populations," *Advances in Space Research*, vol. 41, no. 7, pp. 1046–1053, 2008.

[2] D. J. Kessler, N. L. Johnson, J. Liou, and M. Matney, "The Kessler syndrome: Implications to future space operations," *Advances in the Astronautical Sciences*, vol. 137, no. 8, p. 2010, 2010.

[3] K. Wormnes, R. Le Letty, L. Summerer, R. Schonenborg, O. Dubois-Matra, E. Luraschi, A. Cropp, H. Krag, and J. Delaval, "ESA technologies for space debris remediation," in *6th European Conference on Space Debris*, vol. 1. Noordwijk, The Netherlands: ESA Communications ESTEC, 2013, pp. 1–8.

[4] D. Izzo and M. Märtens, "The Kessler run: On the design of the GTOC9 challenge," *Acta Futura*, vol. 11, pp. 11–24, 2018.

[5] A. Ruggiero, P. Pergola, and M. Andrenucci, "Small electric propulsion platform for active space debris removal," *IEEE Transactions on Plasma Science*, vol. 43, no. 12, pp. 4200–4209, 2015.

[6] D. C. Woffinden and D. K. Geller, "Navigating the road to autonomous orbital rendezvous," *Journal of Spacecraft and Rockets*, vol. 44, no. 4, pp. 898–909, 2007.

[7] L. S. Breger and J. P. How, "Safe trajectories for autonomous rendezvous of spacecraft," *Journal of Guidance, Control, and Dynamics*, vol. 31, no. 5, pp. 1478–1489, 2008.

[8] J. A. Starek, B. Açıkmeşe, I. A. Nesnas, and M. Pavone, "Spacecraft autonomy challenges for next-generation space missions," in *Advances in Control System Technology for Aerospace Applications*. Springer, 2016, pp. 1–48.

[9] U. Eren, A. Prach, B. B. Koçer, S. V. Raković, E. Kayacan, and B. Açıkmeşe, "Model predictive control in aerospace systems: Current state and opportunities," *Journal of Guidance, Control, and Dynamics*, vol. 40, no. 7, pp. 1541–1566, 2017.

[10] A. Richards and J. P. How, "Robust variable horizon model predictive control for vehicle maneuvering," *International Journal of Robust and Nonlinear Control*, vol. 16, no. 7, pp. 333–351, 2006.

[11] S. Di Cairano, H. Park, and I. Kolmanovsky, "Model predictive control approach for guidance of spacecraft rendezvous and proximity maneuvering," *International Journal of Robust and Nonlinear Control*, vol. 22, no. 12, pp. 1398–1427, 2012.

[12] M. Leomanni, E. Rogers, and S. B. Gabriel, "Explicit model predictive control approach for low-thrust spacecraft proximity operations," *Journal of Guidance, Control, and Dynamics*, vol. 37, no. 6, pp. 1780–1790, 2014.

[13] S. S. Farahani, I. Papusha, C. McGhan, and R. M. Murray, "Constrained autonomous satellite docking via differential flatness and model predictive control," in *55th IEEE Conference on Decision and Control*, 2016, pp. 3306–3311.

[14] M. Mammarella, M. Lorenzen, E. Capello, H. Park, F. Dabbene, G. Guglieri, M. Romano, and F. Allgöwer, "An offline-sampling SMPC framework with application to autonomous space maneuvers," *IEEE Transactions on Control Systems Technology*, vol. 28, no. 2, pp. 388–402, 2020.

[15] M. Leomanni, A. Garulli, A. Giannitrapani, and F. Scortecci, "All-electric spacecraft precision pointing using model predictive control," *Journal of Guidance, Control, and Dynamics*, vol. 38, no. 1, pp. 161–168, 2015.

[16] C. Gazzino, D. Arzelier, C. Louembet, L. Cerri, C. Pittet, and D. Losa, "Long-term electric-propulsion geostationary station-keeping via integer programming," *Journal of Guidance, Control, and Dynamics*, vol. 42, no. 5, pp. 976–991, 2019.

[17] W. Fehse, *Automated Rendezvous and Docking of Spacecraft*. Cambridge University Press, 2003.

[18] M. Leomanni, A. Garulli, A. Giannitrapani, and R. Quartullo, "Satellite relative motion modeling and estimation via nodal elements," *Journal of Guidance, Control, and Dynamics*, 2020, article in advance.

[19] M. Leomanni, G. Bianchini, A. Garulli, and A. Giannitrapani, "State feedback control in equinoctial variables for orbit phasing applications," *Journal of Guidance, Control, and Dynamics*, vol. 41, no. 8, pp. 1815–1822, 2018.

[20] S. a. Keerthi and E. G. Gilbert, "Optimal infinite-horizon feedback laws for a general class of constrained discrete-time systems: Stability and moving-horizon approximations," *Journal of Optimization Theory and Applications*, vol. 57, no. 2, pp. 265–293, 1988.

[21] M. Leomanni, G. Bianchini, A. Garulli, A. Giannitrapani, and R. Quartullo, "Sum-of-norms model predictive control for spacecraft maneuvering," *IEEE Control Systems Letters*, vol. 3, no. 3, pp. 649–654, 2019.

[22] M. Leomanni, A. Garulli, A. Giannitrapani, and F. Scortecci, "Propulsion options for very low Earth orbit microsatellites," *Acta Astronautica*, vol. 133, pp. 444–454, 2017.